Energy 70 (2014) 79–85

Contents lists available at ScienceDirect

Energy

journal homepage: www.elsevier.com/locate/energy

Evaluation of temperature-dependent thermoelectric performances based on $PbTe_{1-y}I_y$ and PbTe: Na/Ag_2Te materials

Shanhe Su, Tie Liu, Junyi Wang, Jincan Chen*

Fujian Key Laboratory of Semiconductor Materials and Applications and Department of Physics, Xiamen University, Xiamen 361005, People's Republic of China

ARTICLE INFO

Article history:
Received 3 August 2013
Received in revised form
13 January 2014
Accepted 22 March 2014
Available online 21 April 2014

Keywords:
Thermoelectric device
Temperature-dependent material
Domenicali's equation
Finite difference method
Structure parameter design

ABSTRACT

With the help of Domenicali's equation and the heat flux equation, a finite difference method is directly used to determine the temperature and heat flux distribution profiles in one dimension of a thermoelectric generator simultaneously including the Peltier, Fourier, Joule, and Thomson effects. This calculative method is also used to evaluate the performance of a thermoelectric generator, based on experimental data of thermoelectric materials $PbTe_{1-y}I_y$ and PbTe: Na/Ag_2Te. The efficiency of the thermoelectric generator as a function of the electric current is calculated and the effects of structure parameters on the performance of the thermoelectric generator are revealed. The method proposed here offers a simple way to properly choose n-type and p-type thermoelectric materials of a thermoelectric generator.

1. Introduction

Developing renewable energy and improving the energy conversion efficiency are of important topics for a sustainable future with the development of human activities [1–3]. Semiconductor thermoelectric generators (TEGs) can convert an enormous amount of unused waste heat to electricity and is expected to play an important role in the global sustainable energy issue [4]. Compared with the conventional energy conversion devices, thermoelectric systems have obvious advantages, such as no moving part, quite, compact and reliable for long term supply [5–7]. TEGs have been widely used in many fields. For example, a solar-driven TEG, which consists of a TEG and a solar collector, has the potential to partly convert solar energy into electricity under terrestrial operation condition [8,9]. In Ref. [10], a proof of the principle experiment has been designed to demonstrate that the solar-driven TEG is a new approach of capturing solar energy. Besides, a TEG can be integrated into the bottom of a top system, such as photovoltaic modules [11], thermophotovoltaic cells [12,13], engine cycles [14,15], and fuel cells [16], to recover waste heat, which is another promising way for energy conversion efficiency enhancement.

The energy conversion efficiency of TEGs is mainly determined by the figure of merit ZT, which is closely dependent on the Seebeck coefficient S, electrical resistivity ρ, thermal conductivity κ, and defined as $ZT = S^2T/(\kappa\rho)$ [17]. Nowadays, the theoretical and experimental researches are mostly focusing on increasing the figure of merit ZT. Venkatasubramanian et al. reported that a p-type Bi_2Te_3/Sb_2Te_3 has $ZT \approx 2.4$ at room temperature by controlling the transport of phonons and electrons in the superlattices [18]. By combination of sub-atomic-per-cent doping and nanostructuring, Mehta et al. observed that bulk nanomaterials exhibit higher ZT than their non-nanostructured bulk counterparts [19]. Sevinçli showed through calculation that zigzag graphene nanoribbons are very promising materials for thermoelectric applications [20]. It has been found from the figures in Refs. [21–25] that the Seebeck coefficient S, electrical resistivity ρ, and thermal conductivity κ of thermoelectric materials are functions of temperature. It shows clearly that the effects of temperature on the material properties should be taken into account when the performance of the thermoelectric devices is evaluated. However, only a few researchers considered these effects. Domenicali first built the partial differential equation through the thermodynamic theory of irreversible processes to find the stationary temperature distribution in an electrically heated conductor for given boundary condition [26]. Mahan pointed out that Domenicali's equation and a heat flux equation must be used to calculate the efficiency of a TEG when transport coefficients vary with temperature [27]. This method

* Corresponding author.
E-mail addresses: shanhesu@gmail.com (S. Su), jcchen@xmu.edu.cn (J. Chen).

http://dx.doi.org/10.1016/j.energy.2014.03.090
0360-5442/

allows the efficiency to be evaluated when a thermoelectric device is imposed any configuration of doping. Hogan and Shih derived an iterative technique based on Mahan's equations. A comparison between the results from the iterative technique and the exact approach showed to be in agreement with each other [28]. Yamashita studied the effects of linear and non-linear components in temperature dependence thermoelectric properties on the cooling performance [29]. The temperature dependence of material properties were also considered in solar TEG systems. Li et al. put forward a discrete numerical model to design a concentration solar TEG [30]. Kraemer simulated the performance of a flat-panel solar TEG, based on the best available properties of various bulk thermoelectric materials reported in the literature. The best possible conversion efficiency of solar TEGs was calculated and was highly consistent with the experimental measurement [1]. Xiao et al. revealed that thermal design for a solar-driven TEG could take full advantages of the characteristics of thermoelectric materials and effectively improve the performance [31].

In this article, a governing equation using finite difference method for temperature in one dimension of a TEG is originally derived by employing Domenicali's equation and the heat flux equation. This calculative method has quick convergence and capability of searching the optimal solution within defined space. Based on the experimental characteristics of the temperature-dependent Seebeck coefficient, electrical resistivity, and thermal conductivity of samples $PbTe_{1-y}I_y$ and PbTe: Na/Ag_2Te, the temperature and heat flux distribution profiles are determined numerically. The efficiency of a TEG as a function of the current density is calculated and the TEG is optimally designed. The effects of structure parameters on the performance of the TEG are revealed. When material properties are independent of temperature, the performance of the TEG can be simultaneously discussed by using both the analytical method and the finite difference method.

2. Governing equations for a thermoelectric generator and finite difference method

Fig. 1 shows the schematic diagram of a TEG. The length of the device is L. The forward direction is defined from the cold end to the hot end. T_c is the cold temperature of the device at position $x = 0$. T_h is the hot temperature of the device at position $x = L$. J_p and J_n are the current densities of the p- and n-type legs. The right hand side of Fig. 1 shows the control volume i for a 1-D slab, represented by Δx at position x. The interior nodal i is assumed to have a constant temperature $T_{\lambda,i}$. $q_{\lambda,i}$ and $q_{\lambda,i-1}$ are the net heat flux densities into nodals i and $i-1$ for one leg, where the subscripts $\lambda = n$ and p represent the n- and ptype materials.

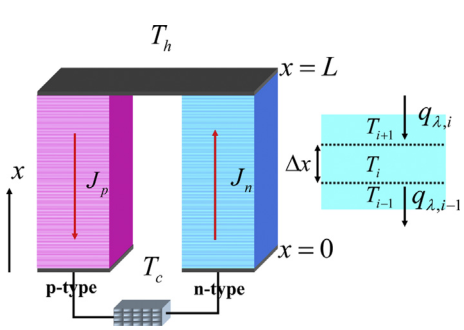

Fig. 1. The schematic diagram of a thermoelectric generator and the control volume for a 1-D slab.

For a thermoelectric device, Domenicali's equation is a well known equation to describe energy flux balance over a segment of a discretized thermoelectric element at position x [27,28,32,33] and is given by

$$\frac{\partial}{\partial x}\left(\kappa_\lambda(x)\frac{\partial T_\lambda(x)}{\partial x}\right) = -\rho_\lambda(x)J_\lambda^2 + J_\lambda T_\lambda(x)\frac{\partial S_\lambda(x)}{\partial x}; (\lambda = n, p), \tag{1}$$

where $\kappa_\lambda(x)$ is the thermal conductivity, $T_\lambda(x)$ is the temperature, $\rho_\lambda(x)$ is the electrical resistivity, and $S_\lambda(x)$ is the Seebeck coefficient along the leg. These quantities are functions of position x as the temperature varies along the leg. The heat flux density equation at position x is given by Refs. [27,28]

$$q_\lambda(x) = J_\lambda T_\lambda(x)S_\lambda(x) - \kappa_\lambda(x)\frac{\partial T_\lambda(x)}{\partial x}; (\lambda = n, p), \tag{2}$$

where the first term indicates the Peltier effect and the second term denotes the heat conduction.

When the Thomson effect appearing in the thermoelectric device is considered, Eqs. (1) and (2) cannot be exactly solved through the analytic method. To solve Eqs. (1) and (2), the first-order approximation is adopted, which is similar to Refs. [27,28]. Governing equations for temperature should be derived using energy balance conservation over the control volume of a half grid interval width [34]. The finite difference method adopted below will be proved to be an effective method of searching the optimal solution.

Equations (1) and (2) can be converted into

$$\frac{dT_\lambda(x)}{dx} = c_{\lambda 1}(x)T_\lambda(x) + c_{\lambda 2}(x)q_\lambda(x); (\lambda = n, p) \tag{3a}$$

and

$$\frac{dq_\lambda(x)}{dx} = c_{\lambda 3}(x)T_\lambda(x) + c_{\lambda 4}(x)q_\lambda(x) + c_{\lambda 5}(x); (\lambda = n, p), \tag{3b}$$

where $c_{\lambda 1}(x) = J_\lambda S_\lambda(x)/\kappa_\lambda(x)$, $c_{\lambda 2}(x) = -1/\kappa_\lambda(x)$, $c_{\lambda 3}(x) = J_\lambda^2 S_\lambda^2(x)/\kappa_\lambda(x)$, $c_{\lambda 4}(x) = -J_\lambda S_\lambda(x)/\kappa_\lambda(x)$, and $c_{\lambda 5}(x) = \rho_\lambda(x)J_\lambda^2(x)$.

By employing one dimensional finite difference method, Eqs. (3a) and (3b) can be written as

$$\frac{T_{\lambda i} - T_{\lambda i-1}}{\Delta x} = c_{\lambda 1,i}T_{\lambda i} + c_{\lambda 2,i}q_{\lambda i}; (\lambda = n, p) \tag{4a}$$

and

$$\frac{q_{\lambda i+1} - q_{\lambda i}}{\Delta x} = c_{\lambda 3,i+1}T_{\lambda i+1} + c_{\lambda 4,i+1}q_{\lambda i+1} + c_{\lambda 5,i+1}; (\lambda = n, p) \tag{4b}$$

at nodal i. By using Eq. (4a), the heat flux densities into nodals i and $i + 1$ for one leg can be expressed as

$$q_{\lambda i} = \frac{1 - c_{\lambda 1,i}\Delta x}{c_{\lambda 2,i}\Delta x}T_{\lambda i} - \frac{1}{c_{\lambda 2,i}\Delta x}T_{\lambda i-1}; (\lambda = n, p) \tag{5a}$$

and

$$q_{\lambda i+1} = \frac{1 - c_{\lambda 1,i+1}\Delta x}{c_{\lambda 2,i+1}\Delta x}T_{\lambda i+1} - \frac{1}{c_{\lambda 2,i+1}\Delta x}T_{\lambda i}; (\lambda = n, p). \tag{5b}$$

By using equations above, the terms of heat flux densities can be eliminated and the governing equation for the temperature $T_{\lambda,i}$ at nodal i is expressed as

$$a_{\lambda 1}T_{\lambda,i-1} + a_{\lambda 2}T_{\lambda,i} + a_{\lambda 3}T_{\lambda,i+1} = b_\lambda; (\lambda = n, p), \tag{6}$$

where $b_\lambda = c_{\lambda 5,i+1}\Delta x$, $a_{\lambda 1} = 1/c_{\lambda 2,i}\Delta x$, $a_{\lambda 2} = (c_{\lambda 4,i+1}/c_{\lambda 2,i+1}) - (1/c_{\lambda 2,i+1}\Delta x) - (1 - c_{\lambda 1,i}\Delta x/c_{\lambda 2,i}\Delta x)$, and $a_{\lambda 3} = (1 - c_{\lambda 1,i+1}\Delta x/c_{\lambda 2,i+1}\Delta x) \quad -c_{\lambda 3,i+1}\Delta x - ((1 - c_{\lambda 1,i+1}\Delta x)c_{\lambda 4,i+1}/c_{\lambda 2,i+1})$. $c_{\lambda m,i}(m = 1 \sim 5)$ are the material properties defined in Eq. (3). In this paper, the Dirichlet boundary condition is used. It means that the temperatures on two sides of the device are fixed [34]. Eq. (6) can be applied to each segment and iteratively solved until the desired temperature profile is obtained.

On the basis of the determination of the temperature and heat flux characteristics, the efficiencies of the n- and p-type legs are given by Refs [28,33]

$$\eta_\lambda = \frac{J_\lambda\left(\int_0^L S_\lambda(x)\frac{\mathrm{d}T_\lambda(x)}{\mathrm{d}x}\mathrm{d}x + J_\lambda\int_0^L \rho_\lambda(x)\mathrm{d}x\right)}{q_\lambda(L)}; (\lambda = n, p) \tag{7}$$

and the total efficiency of the TEG is given by Ref. [28]

$$\eta = \frac{\eta_p\left(\frac{q_p(L)}{J_p}\right) - \eta_n\left(\frac{q_n(L)}{J_n}\right)}{\left(\frac{q_p(L)}{J_p}\right) - \left(\frac{q_n(L)}{J_n}\right)}. \tag{8}$$

In Fig. 2 (a) and (b), efficiencies for the p-type and n-type legs are calculated. Thermoelectric properties can be found by examples from Chapter 12 in Ref. [35], where the Seebeck coefficient S, electrical resistivity ρ, and thermal conductivity κ as a function of temperature are, respectively, given by $S_p = 0.150T + 211(\mu\mathrm{V/K})$, $\rho_p = 1/25(\Omega\mathrm{cm})$, and $\kappa_p = 3.194/T(\mathrm{W/cmK})$ for the p-type leg and $S_n = 0.268T{-}329(\mu\mathrm{V/K})$, $\rho_n = 0.1746/(T{-}310)(\Omega\mathrm{cm})$, and $\kappa_n = 54/T(\mathrm{W/cmK})$ for the n-type leg. The results show that there is no difference between the calculated curves of the present method and those of Ref. [35]. It demonstrates the validity of the present method. The main advantage of the present method is to simplify calculation, so that the numerical solution of a governing equation, such as Eq. (6), can converge in a matter of seconds. Thus, the present method opens a more efficient way to solve a similar problem.

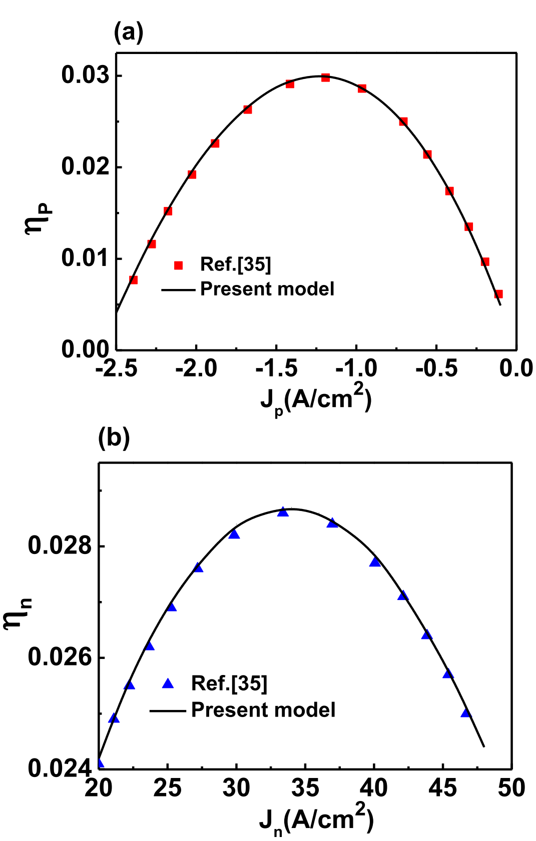

Fig. 2. Comparison between the curves obtained by Ref. [35] and the present method for given examples of (a) p-type material and (b) n-type material.

In this paper, only steady-state behavior is studied. An important feature of the model is its ability to calculate the temperature profile taking the real temperature-dependent properties of thermoelectric materials into account. This feature is essential in evaluating the performance of a TEG exposed to a given temperature difference.

3. Properties of temperature-dependent thermoelectric materials

In this article, the n- and p-type materials, $PbTe_{1-y}I_y$ [22] and PbTe: Na/Ag_2Te [23], are selected to evaluate the performance of a TEG, because these materials have similar temperature-dependent characteristics and relatively large figures of merit ZT. With the coupling of large nanostructures and complex band structures, PbTe: Na/Ag_2Te becomes a high performance thermoelectric material. The inclusion of Ag_2Te in PbTe reduces the lattice thermal conductivity by providing scattering phonons through nanostructuring. The doping of Na creates multiple bands to enhance the Seebeck coefficient by improving electronic properties [23]. For $PbTe_{1-y}I_y$, Aaron et al. revealed that ZT of materials $PbTe_{1-y}I_y$ can attain *1.4* at high temperatures with precisely doping control [22]. Fig. 3 summarizes the experimental characteristics of the temperature-dependent Seebeck coefficient S, electrical resistivity ρ, and thermal conductivity κ for different n-type samples $PbTe_{1-y}I_y$ ($y = 0.0004$, 0.0007, 0.0012, 0.0020, 0.0028, 0.0040, 0.0055 and 0.0100) [22] and the temperature-dependent Seebeck coefficient S, electrical resistivity ρ, and figure of merit ZT for p-type materials PbTe: Na/Ag_2Te with different contents of Na [23]. As can be seen from Fig. 3 (a), the absolute Seebeck coefficient and electrical resistivity increase with lower doping of I, while the thermal conductivity monotonically decreases. These suggest that the doping of I should be optimally selected when $PbTe_{1-y}I_y$ is used as a thermoelectric element. From Fig. 3 (b), it can be found that *ZT* of PbTe: Na/Ag_2Te increases with the larger content of Na over the entire temperature range, because the electrical resistivity is significantly reduced by increasing the content of Na while the Seebeck coefficient and thermal conductivity are roughly unchanged. The thermal conductivity of PbTe: Na/Ag_2Te can be calculated from $\kappa = S^2T/(\rho ZT)$. On the basis of Fig. 3, the efficiency of the TEG will be evaluated and the TEG will be optimally designed in the following section.

4. Performance evaluation and structure optimum design

PbTe based thermoelectric materials usually have high performance at middle temperature range (*600–850 K*) [36]. Because the regions of temperatures given in Fig. 3 are mostly between *300 K* and *700 K*, it is adopted in the following discussions that the cold end temperature T_c is *300 K* and hot end temperature is *700 K*. These boundary conditions are used for both n-type and p-type materials unless specifically mentioned. Based on Eq. (7) and experimental data of n-type materials $PbTe_{1-y}I_y$ in Fig. 3 (a), the efficiency η_n as a function of the current density J_n is plotted, as shown in Fig. 4 (a). The length of the leg is 1 cm. Fig. 4 (a) shows that the efficiency η_n is

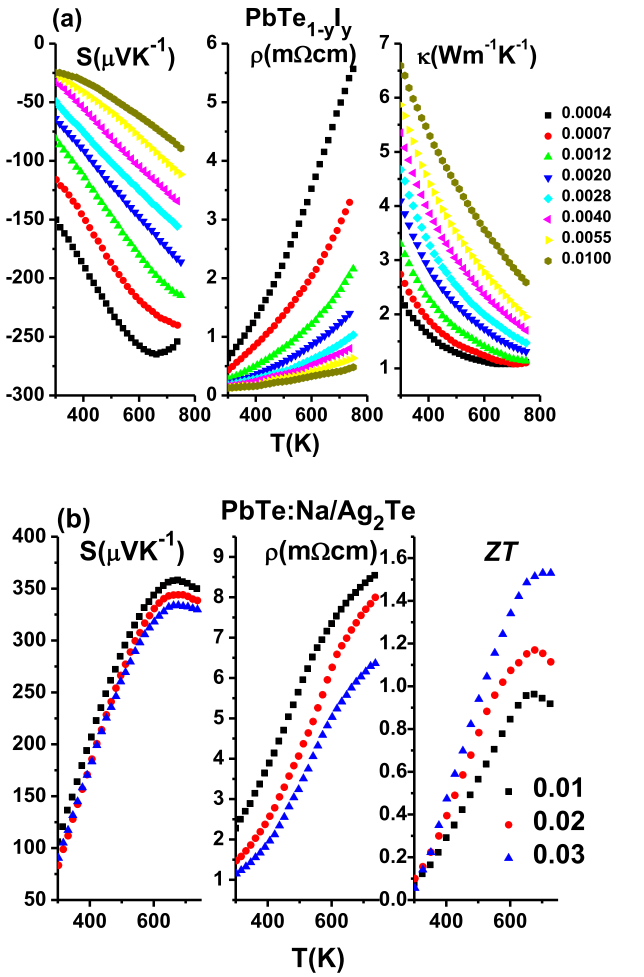

Fig. 3. Experimental characteristics of the temperature-dependent Seebeck coefficient, electrical resistivity, and (a) thermal conductivity for n-type materials $PbTe_{1-y}I_y$ [22] for different samples (x = 0.0004, 0.0007, 0.0012, 0.0020, 0.0028, 0.0040, 0.0055 and 0.0100), and (b) figure of merit for p-type materials PbTe: Na/Ag_2Te [23] for different contents of Na.

not a monotonic function of the current density J_n. η_n attains a maximum value when J_n is adjusted to a reasonable value. Generally, the voltage of the thermoelectric generator decreases whereas the current density increases, suggesting an optimal value for power conversion efficiency. Fig. 4 (a) also shows that the largest efficiency $\eta_{n,max}$ is achieved for the sample with $y = 0.0007$, because this sample has relatively larger ZT over the entire temperature range along the thermoelectric leg. Fig. 4 (b) shows the efficiency η_p as a function of the current density J_p for p-type materials PbTe: Na/Ag_2Te for different contents of Na. J_p is negative for the forward direction defined in Fig. 1. According to Fig. 4 (b), the largest efficiency $\eta_{p,\max}$ is obtained for the sample having the content, *0.03*, of Na, because ZT of PbTe: Na/Ag_2Te increases with the increasing content of Na. The samples $PbTe_{0.9993}I_{0.0007}$ and PbTe: Na/Ag_2Te with the content, *0.03*, of Na will be used to evaluate the performance and design the structure of a TEG.

According to Eqs. (5) and (6) and the numerical method mentioned in the second section, the temperature and heat flux as a function of the position for n- and p-type legs can be obtained. Fig. 5 shows the temperature versus position curves for samples $PbTe_{0.9993}I_{0.0007}$ and PbTe: Na/Ag_2Te. Fig. 6 shows the heat flux versus position curves for samples $PbTe_{0.9993}I_{0.0007}$ and PbTe: Na/Ag_2Te. The current densities of n- and p-type legs are $J_p = -12A/\text{cm}^2$ and $J_n = 20A/\text{cm}^2$. It can be seem from Fig. 5 that the temperature profiles of two materials are similar and not a linear function of position. It is because the non-linear characteristics in the temperature dependences of thermoelectric properties cause non-uniform distribution of heat generation and consumption along the thermoelectric leg. Fig. 6 displays that the absolute value of the heat flux decreases as the position is away from the hot end because more thermal energy is converted to electric energy.

According to Eq. (8), the efficiency η of the TEG can be calculated, as shown in Fig. 7, where the cross sectional area of the p-type leg is assumed to be 1 cm^2 and the cross sectional area of the n-type leg is 1/3 cm^2. Fig. 7 shows that the efficiency η increases as the current I increases, but after reaching a maximum point, it decreases as the current I further increases. The reason is similar to Fig. 4 (a) and can be explained by the current voltage characteristics of a TEG. As the current increases, more heat is converted to electricity by the Peltier effect, but η can not infinitely increase because of the reduction of voltage. The maximal value $\eta_{\max}$ of the efficiency is larger than *10%*, as shown in Fig. 7. The efficiency can be further improved if the structure of the TEG is optimally designed.

According to Eq. (8) and Fig. 7, the optimization analysis is applied to discuss the cross sectional area effects on the performance of TEG, as shown in Fig. 8, where the horizontal coordinate is the cross sectional area A_n of the n-type leg while the cross sectional area of the p-type leg equals 1 cm^2. In Fig. 8, the efficiency η_{opt,A_n} has been maximized with respect to the current. It is worthwhile to point out that η_{opt,A_n} is not a monotonically increasing function of A_n. η_{opt,A_n} increases with the increase of A_n when A_n is small. However, η_{opt,A_n} attains its maximum $(\eta_{opt,A_n})_{\max}$ when $A_n = A_{n,m}$. If A_n further increases, η_{opt,A_n} will decrease.

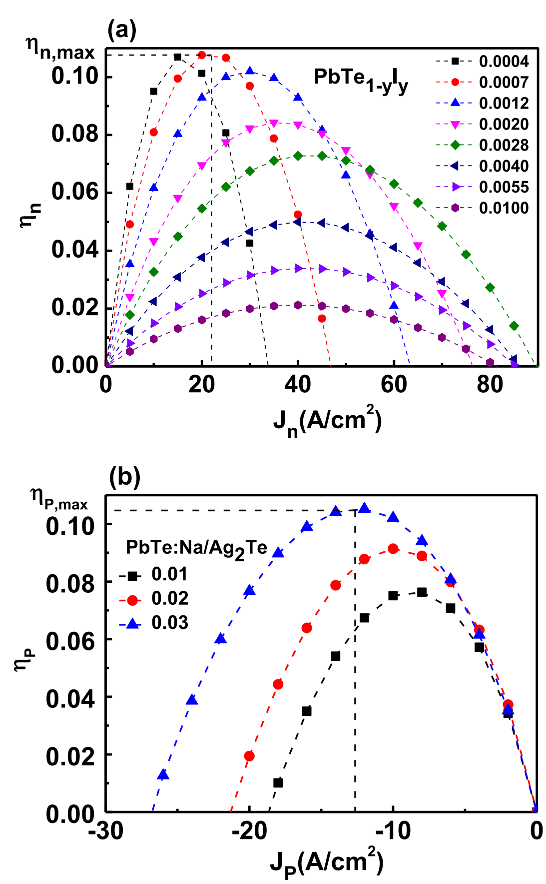

Fig. 4. Efficiency versus current density curves for (a) n-type materials $PbTe_{1-y}I_y$ and (b) p-type materials PbTe: Na/Ag_2Te.

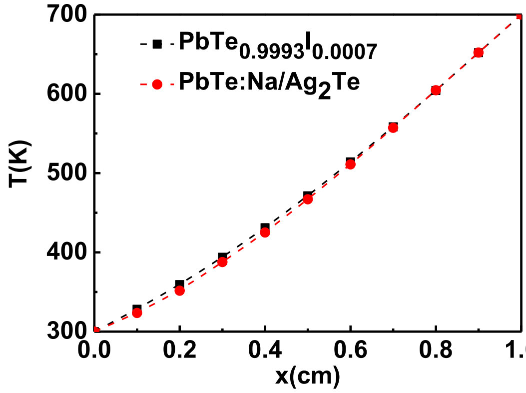

Fig. 5. Temperature versus position curves for samples $PbTe_{0.9993}I_{0.0007}$ and PbTe: Na/Ag_2Te.

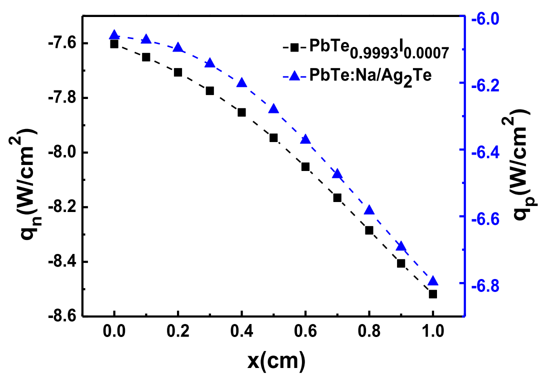

Fig. 6. Heat flux versus position curves for samples $PbTe_{0.9993}I_{0.0007}$ and PbTe: Na/Ag_2Te.

5. Two calculative methods of a simplified model

In order to conveniently determine the performance of a TEG, a simplified method is often used [35,37,38] by assuming that the Seebeck coefficient, electrical resistivity, and thermal conductivity of the TEG are independent of temperature. In such a case, the Thomson coefficient equals zero, i.e., $T(x)dS_\lambda(x)/dT = 0;(\lambda = n,p)$. Eq. (1) can be simplified into [35]

$$\kappa_\lambda \frac{d^2 T_\lambda(x)}{dx^2} = -\rho_\lambda J_\lambda^2; (\lambda = n, p). \tag{9}$$

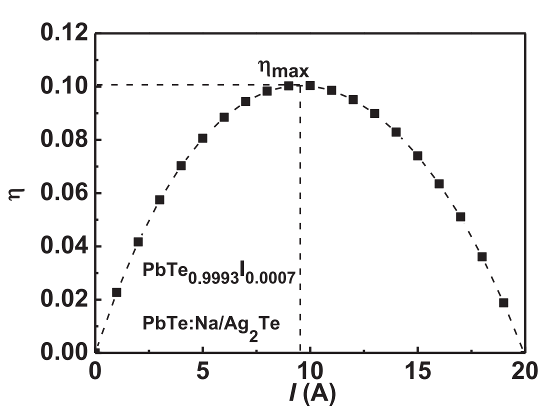

Fig. 7. The efficiency η versus current I curve of the thermoelectric generator consisting of $PbTe_{0.9993}I_{0.0007}$ and PbTe: Na/Ag_2Te.

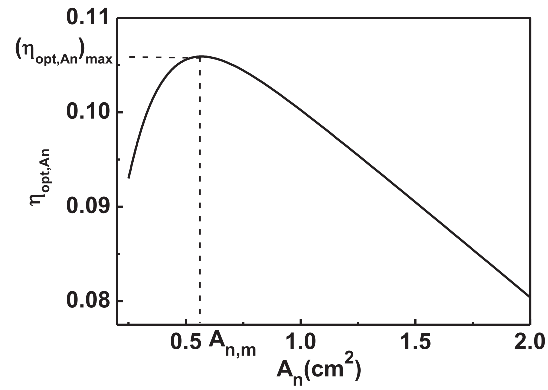

Fig. 8. The curve of the efficiency η of a thermoelectric generator varying with the cross sectional area A_n of the n-type leg.

By using the boundary condition $T_\lambda(0) = T_c$ and $T_\lambda(L) = T_h$, Eq. (9) can be integrated to obtain

$$\kappa_\lambda \frac{dT_\lambda(x)}{dx} = -\rho_\lambda J_\lambda^2 (x - L/2) + \frac{\kappa_\lambda (T_c - T_h)}{L}; (\lambda = n, p). \tag{10}$$

Using Eqs. (2) and (10), one can derive the heat flow densities at $x = 0$ and $x = L$ as

$$q_\lambda(0) = J_\lambda T_c S_\lambda - \rho_\lambda J_\lambda^2 L\big/2 + \frac{\kappa_\lambda (T_h - T_c)}{L}; (\lambda = n, p) \tag{11}$$

and

$$q_\lambda(L) = J_\lambda T_h S_\lambda + \rho_\lambda J_\lambda^2 L\big/2 + \frac{\kappa_\lambda (T_h - T_c)}{L}; (\lambda = n, p). \tag{12}$$

It can be derived from Eqs. (11) and (12) that the total heat flows from the hot end to the TEG and from the TEG to the cold end are, respectively, given by

$$q_h = SI_a T_h - \frac{1}{2} I_a^2 R + K(T_h - T_c) \tag{13}$$

and

$$q_c = SI_a T_c + \frac{1}{2} I_a^2 R + K(T_h - T_c), \tag{14}$$

where $S = (S_p - S_n)$, $R = (\rho_p L/A_p + \rho_n L/A_n)$, and $K = (\kappa_p A_p/L + \kappa_n A_n/L)$ are the Seebeck coefficient S, electrical resistance R, and thermal

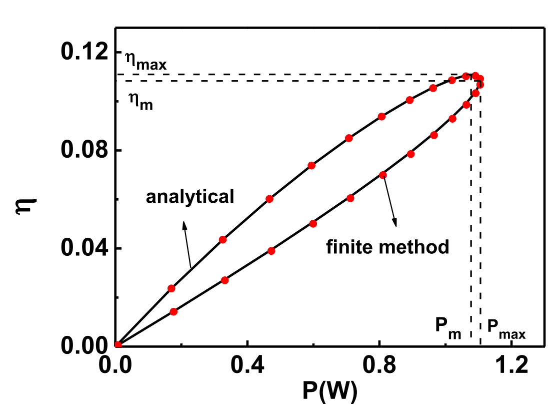

Fig. 9. The efficiency η versus power output curve of the TEG, where the dots on the curve are obtained by the finite difference method.

conductance K of a thermoelectric device, and $I_a = J_\lambda A_\lambda$ is the electric current of a TEG. By using Eqs. (13) and (14), the power output P_a and efficiency η_a of the TEG can be analytically expressed as

$$P_a = q_h - q_c = SI_a(T_h - T_c) - I_a^2 R \tag{15}$$

and

$$\eta_a = \frac{P_a}{q_h} = \frac{SI_a(T_h - T_c) - I_a^2 R}{SI_a T_h - \frac{1}{2}I_a^2 R + K(T_h - T_c)}. \tag{16}$$

Fig. 9 shows the efficiency η as a function of the power output P obtained from Eqs. (15) and (16), where the dots on the curve are obtained by the finite difference method. In Fig. 9, the cross sectional area of the p-type leg is 1 cm^2, the cross sectional area of the n-type leg is 0.5 cm^2, and the average values of the experimental data of samples $PbTe_{0.9993}I_{0.0007}$ and PbTe: Na/Ag_2Te obtained from Fig. 3, which are listed in Table 1, are adopted. It is seen from Fig. 9 that the results obtained by two calculative methods are identical. The calculations of error analysis by the finite difference method and the analytical method are also shown in Table 2. The error is quantified as a percent discrepancy, which is the ratio of the efficiency difference between the finite difference method and the analytical method to the efficiency calculated by finite difference method. The largest error is only *1.68%* at current *25A*. In addition, Fig. 9 shows that the $\eta \sim P$ curve is a closed loop line passing through the zeros point. On the curve, there are a maximum efficiency $\eta_{\max}$, whose corresponding power output is P_m, and a maximum power output $P_{\max}$ whose corresponding efficiency is η_m. Thus, the ranges of the efficiency and the power output must be constrained by $\eta_m \le \eta \le \eta_{\max}$ and $P_m \le P \le P_{\max}$. Obviously, $\eta_{\max}$ and $P_{\max}$ determine the upper bounds of the efficiency and power output, while η_m and P_m give the lower bounds of the optimized efficiency and power output. Thus, $\eta_{\max}$, $P_{\max}$, η_m, and P_m are some four important parameters of TEGs.

6. Conclusions

With the help of Domenicali's equation and heat flux equation, a finite difference method is directly used to determine the temperature and heat flux distribution profiles of a thermoelectric generator in one dimension. Efficiencies of the thermoelectric generator under different conditions are calculated based on experimental characteristics of the temperature-dependent Seebeck coefficient, electrical resistivity, and thermal conductivity for samples $PbTe_{1-y}I_y$ and PbTe: Na/Ag_2Te. The efficiency and structure parameter are optimally designed. It is proved that the finite difference method adopted here is accurate and quick convergence to evaluate the performance of the TEG by comparing with other methods. The method offers a simple way to properly choose thermoelectric elements of a thermoelectric generator on the basis of the experimental characteristics of thermoelectric properties.

Table 1
The average values of temperature-dependent material parameters for samples $PbTe_{0.9993}I_{0.0007}$ and PbTe: Na/Ag_2Te.

Sample	Type	α (μV/K)	ρ (mΩ cm)	κ (W/m-K)
$PbTe_{0.9993}I_{0.0007}$	n	−189	1.67	1.53
$PbTe:Na/Ag_2Te$	p	253	3.72	0.947

Table 2
The calculations of error analysis by the finite difference method and the analytical method.

Current (A)	Finite method	Analytical method	Error (%)
	Efficiency	Efficiency	
1	0.0237	0.0237	0
4	0.0738	0.0739	0.136
10	0.110	0.111	0.909
12	0.109	0.110	0.917
17	0.0862	0.0870	0.928
19	0.0699	0.0707	1.14
22	0.0390	0.0395	1.28
25	0.000595	0.000605	1.68

Acknowledgments

This work has been supported by the National Natural Science Foundation (No. 11175148), 973 Program (No. 2012CB619301), and the Fundamental Research Fund for the Central Universities (No. 201312G007), People's Republic of China.

Nomenclature

S	Seebeck coefficient (μV K^{-1})
ZT	figure of merit
x	position along TEG
L	length of TEG
T_c	cold end temperature
T_h	hot end temperature
J_p	current density of p-type leg
J_n	current density of n-type leg
Δx	control volume
$T_{\lambda,i}$	temperature at nodal i
$q_{\lambda,i}$	heat flux density into nodal i
$T_\lambda(x)$	temperature at x
$q_\lambda(x)$	heat flux density at x
$c_{\lambda m,i}(m = 1 \sim 5)$	material properties defined in Eq. (3)
$a_{\lambda 1}, a_{\lambda 2}, a_{\lambda 3}$	factor of the matrix defined in Eq. (6)
b_λ	factor of the matrix defined in Eq. (6)
A_n	cross sectional area of n type leg
R	electrical resistance
K	thermal conductance
I	electric current
P_m	power at maximum efficiency

Greek symbols

ρ	electrical resistivity (mΩ cm)
κ	thermal conductivity (Wm^{-1} K^{-1})
η_λ	efficiencies of n- or p-type legs
η	total efficiency
η_m	efficiency at maximum power

Superscripts and subscripts

h	hot end of TEG
c	cold end of TEG
i	interior nodal along TEG
n	n-type
p	p-type
λ	n or p type material
max	maximum value
opt	optimal value
y	different samples of $PbTe_{1-y}I_y$
a	a parameter independent of temperature

Abbreviations

TEG thermoelectric generator

References

[1] Dahl S, Chorkendorff I. Solar–fuel generation: towards practical implementation. Nat Mater 2012;11:100–1.

[2] Cheng TC, Cheng CH, Huang ZZ, Liao GC. Development of an energy-saving module via combination of solar cells and thermoelectric coolers for green building applications. Energy 2011;36:133–40.

[3] Shu G, Zhao J, Tian H, Liang X, Wei H. Parametric and exergetic analysis of waste heat recovery system based on thermoelectric generator and organic rankine cycle utilizing R123. Energy 2012;45:806–16.

[4] Snyder GJ, Toberer ES. Complex thermoelectric materials. Nat Mater 2008;7:105–14.

[5] Huang YX, Wang XD, Cheng CH, Lin DT. Geometry optimization of thermoelectric coolers using simplified conjugate-gradient method. Energy 2013;59:689–97.

[6] Martínez A, Astrain D, Rodríguez A. Dynamic model for simulation of thermoelectric self cooling applications. Energy 2013;55:1114–26.

[7] Qiu K, Hayden ACS. A Natural–gas–fired thermoelectric power generation system. J Electron Mater 2009;38:1315–9.

[8] Chen J. Thermodynamic analysis of a solar-driven thermoelectric generator. J Appl Phys 1996;79:2717–21.

[9] Chen G. Theoretical efficiency of solar thermoelectric energy generators. J Appl Phys 2011;109:104908.

[10] Kraemer D, Poudel B, Feng HP, Caylor JC, Yu B, Yan X, et al. High–performance flat–panel solar thermoelectric generators with high thermal concentration. Nat Mater 2011;10:532–8.

[11] Sark W. Feasibility of photovoltaic – thermoelectric hybrid modules. Appl Energy 2011;88:2785–90.

[12] Qiu K, Hayden ACS. Development of a novel cascading TPV and TE power generation system. Appl Energy 2012;91:304–8.

[13] Srivastava A, Pinder M, Shah S, Raghav V, Komerath N. Thermoelectric and thermophotovoltaic micro renewable power systems for home use. 10th International Energy Conversion Engineering Conference Atlanta, Georgia, 30 July – 01 August 2012, DOI: 10.2514/6.2012-3900.

[14] Sahin AZ, Yilbas BS, Shuja SZ, Momin O. Investigation into topping cycle: thermal efficiency with and without presence of thermoelectric generator. Energy 2011;36:4048–54.

[15] Hsiao YY, Chang WC, Chen SL. A mathematic model of thermoelectric module with applications on waste heat recovery from automobile engine. Energy 2010;35:1447–54.

[16] Chen X, Chen L, Guo J, Chen J. An available method exploiting the waste heat in a proton exchange membrane fuel cell system. Int J Hydrogen Energy 2011;16:6099–104.

[17] Sahin AZ, Yilbas BS. Thermodynamic irreversibility and performance characteristics of thermoelectric power generator. Energy 2013;55:899–904.

[18] Venkatasubramanian R, Siivola E, Colpitts T, O'Quinn B. Thin–film thermoelectric devices with high room–temperature figures of merit. Nature 2001;413:597–602.

[19] Mehta RJ, Zhang Y, Karthik C, Singh B, Siegel RW, Borca–Tasciuc T, et al. A new class of doped nanobulk high–figure–of–merit thermoelectrics by scalable bottom–up assembly. Nat Mater 2012;11:233–40.

[20] Sevinçli H, Cuniberti G. Enhanced thermoelectric figure of merit in edge–disordered zigzag graphene nanoribbons. Phys Rev B 2010;81:113401.

[21] Pei Y, LaLonde A, Iwanaga S, Snyder GJ. High thermoelectric figure of merit in heavy hole dominated PbTe. Energy Environ Sci 2011;4:2085–9.

[22] LaLonde A, Pei Y, Snyder GJ. Reevaluation of $PbTe_{1-x}I_x$ as high performance n–type thermoelectric material. Energy Environ Sci 2011;4:2090–6.

[23] Pei Y, Heinz NA, LaLonde A, Snyder GJ. Combination of large nanostructures and complex band structure for high performance thermoelectric lead telluride. Energy Environ Sci 2011;4:3640–5.

[24] Biswas K, He J, Zhang Q, Wang G, Uher C, Dravid VP, et al. Strained endotaxial nanostructures with high thermoelectric figure of merit. Nat Chem 2011;3:160–6.

[25] Androulakis J, Lee Y, Todorov I, Chung DY. High–temperature thermoelectric properties of n–type PbSe doped with Ga, In, and Pb. Phys Rev B 2011;83:195209.

[26] Domenicali CA. Stationary temperature distribution in an electrically heated conductor. J Appl Phys 1954;25:1310–1.

[27] Mahan GD. Inhomogeneous thermoelectrics. J Appl Phys 1991;70:4551–4.

[28] Rowe DM. Handbook of thermoelectrics: macro to nano. Boca Raton: CRC; 2005.

[29] Yamashita O. Effect of linear and non–linear components in the temperature dependences of thermoelectric properties on the cooling performance. Appl Energy 2009;86:1746–56.

[30] Li P, Cai L, Zhai P, Tang X, Zhang Q, Niino M. Design of a concentration solar thermoelectric generator. J Electron Mater 2010;39:1522–30.

[31] Xiao J, Yang T, Li P, Zhai P, Zhang Q. Thermal design and management for performance optimization of solar thermoelectric generator. Appl Energy 2012;93:33–8.

[32] Chen J, Yan Z, Wu L. The influence of Thomson effect on the maximum power output and maximum efficiency of a thermoelectric generator. J Appl Phys 1996;79:8823–8.

[33] Snyder GJ, Ursell TS. Thermoelectric efficiency and compatibility. Phys Rev Lett 2003;91:148301.

[34] Shih TM. Heat Transfer Lessons with Examples Solved by Matlab. 1st ed. Cognella: Cognella Academic Publishing; 2012.

[35] Rowe DM. Handbook of thermoelectrics. Boca Raton: CRC Press; 1995.

[36] Zhao LD, Lo SH, He J, Li H, Biswas K, Androulakis J, et al. High performance thermoelectrics from earth-abundant materials: enhanced figure of merit in PbS by second phase nanostructures. J Am Chem Soc 2011;133:20476–87.

[37] Chen J, Lin B, Wang H, Lin G. Optimal design of a multi–couple thermoelectric generator. Semicond Sci Technol 2000;15:184–8.

[38] Champier D, Bédécarrats JP, Kousksou T, Rivaletto M, Strub F, Pignolet P. Study of a TE (thermoelectric) generator incorporated in a multifunction wood stove. Energy 2011;36:1518–26.